

# Measurement of $G_{Ep}/G_{Mp}$ in $\vec{e}p \rightarrow e\vec{p}$ to $Q^2 = 5.6 \text{ GeV}^2$

O. Gayou,<sup>1,7</sup> K.A. Aniol,<sup>9</sup> T. Averett,<sup>1</sup> F. Benmokhtar,<sup>2</sup> W. Bertozzi,<sup>24</sup> L. Bimbot,<sup>26</sup> E.J. Brash,<sup>4</sup> J.R. Calarco,<sup>25</sup> C. Cavata,<sup>27</sup> Z. Chai,<sup>24</sup> C.-C. Chang,<sup>23</sup> T. Chang,<sup>15</sup> J.-P. Chen,<sup>5</sup> E. Chudakov,<sup>5</sup> R. De Leo,<sup>16</sup> S. Dieterich,<sup>2</sup> R. Endres,<sup>2</sup> M.B. Epstein,<sup>9</sup> S. Escoffier,<sup>27</sup> K.G. Fissum,<sup>22</sup> H. Fonvieille,<sup>7</sup> S. Frullani,<sup>18</sup> J. Gao,<sup>8</sup> F. Garibaldi,<sup>18</sup> S. Gilad,<sup>24</sup> R. Gilman,<sup>2,5</sup> A. Glamazdin,<sup>21</sup> C. Glashausser,<sup>2</sup> J. Gomez,<sup>5</sup> V. Gorbenko,<sup>21</sup> J.-O. Hansen,<sup>5</sup> D.W. Higinbotham,<sup>24,\*</sup> G.M. Huber,<sup>4</sup> M. Iodice,<sup>17</sup> C.W. de Jager,<sup>5</sup> X. Jiang,<sup>2</sup> M.K. Jones,<sup>5</sup> J.J. Kelly,<sup>23</sup> M. Khandaker,<sup>3</sup> A. Kozlov,<sup>4</sup> K.M. Kramer,<sup>1</sup> G. Kumbartzki,<sup>2</sup> J.J. LeRose,<sup>5</sup> D. Lhuillier,<sup>27</sup> R.A. Lindgren,<sup>26</sup> N. Liyanage,<sup>5</sup> G.J. Lolos,<sup>4</sup> D.J. Margaziotis,<sup>9</sup> F. Marie,<sup>27</sup> P. Markowitz,<sup>12</sup> K. McCormick,<sup>20</sup> R. Michaels,<sup>5</sup> B.D. Milbrath,<sup>11</sup> S.K. Nanda,<sup>5</sup> D. Neyret,<sup>27</sup> Z. Papandreou,<sup>4</sup> L. Pentchev,<sup>1,†</sup> C.F. Perdrisat,<sup>1</sup> N.M. Piskunov,<sup>19</sup> V. Punjabi,<sup>3</sup> T. Pussieux,<sup>27</sup> G. Quéméner,<sup>14</sup> R.D. Ransome,<sup>2</sup> B.A. Raue,<sup>12</sup> R. Roché,<sup>13</sup> M. Rvachev,<sup>24</sup> A. Saha,<sup>5</sup> C. Salgado,<sup>3</sup> S. Širca,<sup>24</sup> I. Sitnik,<sup>19</sup> S. Strauch,<sup>2,‡</sup> L. Todor,<sup>10</sup> E. Tomasi-Gustafsson,<sup>27</sup> G.M. Urciuoli,<sup>18</sup> H. Voskanyan,<sup>29</sup> K. Wijesooriya,<sup>6</sup> B.B. Wojtsekhowski,<sup>5</sup> X. Zheng,<sup>24</sup> L. Zhu<sup>24</sup>

(for the Jefferson Lab Hall A Collaboration)

<sup>1</sup> College of William and Mary, Williamsburg, VA 23187

<sup>2</sup> Rutgers, The State University of New Jersey, Piscataway, NJ 08855

<sup>3</sup> Norfolk State University, Norfolk, VA 23504

<sup>4</sup> University of Regina, Regina, SK S4S 0A2, Canada

<sup>5</sup> Thomas Jefferson National Accelerator Facility, Newport News, VA 23606

<sup>6</sup> Argonne National Laboratory, Argonne, IL 60439

<sup>7</sup> Université Blaise Pascal/CNRS-IN2P3, F-63177 Aubière, France

<sup>8</sup> California Institute of Technology, Pasadena, CA 91125

<sup>9</sup> California State University, Los Angeles, CA 90032

<sup>10</sup> Carnegie-Mellon University, Pittsburgh, PA 15213

<sup>11</sup> Eastern Kentucky University, Richmond, KY 40475

<sup>12</sup> Florida International University, Miami, FL 33199

<sup>13</sup> Florida State University, Tallahassee, FL 32306

<sup>14</sup> Institut des Sciences Nucléaires, CNRS-IN2P3, F-38026 Grenoble, France

<sup>15</sup> University of Illinois, Urbana-Champaign, IL 61801

<sup>16</sup> INFN, Sezione di Bari and University of Bari, 70126 Bari, Italy

<sup>17</sup> INFN, Sezione di Roma-III, 00146 Roma, Italy

<sup>18</sup> INFN, Sezione Sanità and Istituto Superiore di Sanità, 00161 Rome, Italy

<sup>19</sup> JINR-LHE, 141980 Dubna, Moscow Region, Russian Federation

<sup>20</sup> Kent State University, Kent, OH 44242

<sup>21</sup> Kharkov Institute of Physics and Technology, Kharkov 61108, Ukraine

<sup>22</sup> University of Lund, PO Box 118, S-221 00 Lund, Sweden

<sup>23</sup> University of Maryland, College Park, MD 20742

<sup>24</sup> Massachusetts Institute of Technology, Cambridge, MA 02139

<sup>25</sup> University of New Hampshire, Durham, NH 03824

<sup>26</sup> Institut de Physique Nucléaire, F-91406 Orsay, France

<sup>27</sup> DAPNIA/SPHN CEA/Saclay, F-91191 Gif-sur-Yvette, France

<sup>28</sup> University of Virginia, Charlottesville, VA 22901

<sup>29</sup> Yerevan Physics Institute, Yerevan 375036, Armenia

(October 30, 2018)

The ratio of the electric and magnetic form factors of the proton,  $G_{Ep}/G_{Mp}$ , was measured at the Thomas Jefferson National Accelerator Facility (JLab) using the recoil polarization technique. The ratio of the form factors is directly proportional to the ratio of the transverse to longitudinal components of the polarization of the recoil proton in the elastic  $\vec{e}p \rightarrow e\vec{p}$  reaction. The new data presented in this article span the range  $3.5 < Q^2 < 5.6 \text{ GeV}^2$  and are well described by a linear  $Q^2$  fit. Also, the ratio  $QF_{2p}/F_{1p}$  reaches a constant value above  $Q^2 = 2 \text{ GeV}^2$ .

\*Currently at Thomas Jefferson National Accelerator Facility

†On leave of absence from Institute for Nuclear Research and Nuclear Energy, Sofia, Bulgaria

‡Currently at George Washington University, Washington, DC 20052

The nucleon electromagnetic form factors are a key ingredient to describe its internal structure, and eventually understand the strong interaction. Experimental values for the proton have been obtained over the last 50 years via electron-proton scattering, often using the Rosenbluth separation technique [1]. They show that the magnetic form factor,  $G_{Mp}$ , follows approximately a dipole form factor  $G_D = (1 + Q^2/0.71(\text{GeV}^2))^{-2}$  where  $Q^2$  is the four-momentum transfer squared [2–8]. However, measuring the charge form factor  $G_{Ep}$  by Rosenbluth separation becomes difficult for  $Q^2 > 1 \text{ GeV}^2$ , because the charge scattering contributes only little to the differential cross section. Extending the measurement of the form factors to larger  $Q^2$  is important, for example to test the perturbative QCD (pQCD) scaling predictions for the Dirac and Pauli form factors  $F_{1p}$  and  $F_{2p}$  [9]. The recoil polarization method, proposed in the 1970's [10], has been established as the most effective available technique for measuring the ratio  $G_{Ep}/G_{Mp}$  at large  $Q^2$  [11–14]. The results of Ref. [11] showed a surprising, roughly linear, decrease of this ratio as a function of  $Q^2$  up to  $3.5 \text{ GeV}^2$ . In a non-relativistic approach, this faster decrease of  $G_{Ep}$  can be interpreted as confinement of the charge distribution in the Breit frame to a larger region of space than the magnetism distribution.

In the one-photon exchange approximation for elastic  $ep$  scattering, a longitudinally polarized electron beam transfers its polarization to the recoil proton with two non-zero components,  $P_t$ , perpendicular to, and  $P_\ell$ , parallel to, the proton momentum in the scattering plane.  $P_t$  and  $P_\ell$  are proportional to  $G_{Ep}G_{Mp}$  and  $G_{Mp}^2$ , respectively, so that the ratio of the form factors follows directly from the simultaneous measurements of these two polarization components [10]:

$$\frac{G_{Ep}}{G_{Mp}} = -\frac{P_t}{P_\ell} \frac{(E_e + E_{e'})}{2m} \tan \frac{\theta_e}{2} \quad (1)$$

Here  $m$  is the proton mass,  $\theta_e$  is the lab scattering angle, and  $E_e$  and  $E_{e'}$  are the incident and scattered energies of the electron.

We present the results of new measurements of the ratio  $\mu_p G_{Ep}/G_{Mp}$ , where  $\mu_p$  is the magnetic moment of the proton, up to  $Q^2 = 5.6 \text{ GeV}^2$  performed in Hall A at Jefferson Lab. A polarized electron beam from the Continuous Electron Beam Accelerator was scattered on a 15 cm-long circulating liquid hydrogen target. A strained GaAs crystal excited by circularly polarized laser light produced the polarized electron beam, with an average current of  $40 \mu\text{A}$ . A typical longitudinal beam polarization at the target of  $\sim 0.70$  was measured with both a Møller polarimeter [15] (with an uncertainty of  $\sim 3\%$ ) and a Compton polarimeter [16] (with an uncertainty of  $\sim 1.4\%$  [17]). The helicity of the beam was flipped pseudo-randomly at 30 Hz.

Recoil protons were detected in the left high resolution spectrometer (HRS) [18]. The HRS has a central

bend angle of  $45^\circ$ , and accepts a maximum central momentum of  $4 \text{ GeV}/c$  with a  $6.5 \text{ msr}$  acceptance; it has a  $\pm 5\%$  momentum acceptance and a  $< 2 \times 10^{-4}$  momentum resolution. Two vertical drift chambers located at the focal plane, along with the knowledge of the optics of the three quadrupoles and the dipole of the HRS, allow precise position and angle measurements of the proton trajectory at the target. As the data acquisition was triggered by a single proton in the HRS, we also detected the scattered electron in order to isolate elastic  $ep$  scattering events and reject the significant background in the spectrometer, mostly from pion electroproduction. The polarization transfer in this reaction can be different in magnitude and sign from the polarization transfer in elastic scattering.

For the measurement at  $Q^2 = 3.5 \text{ GeV}^2$ , the electron was detected in the second (right) HRS, and the trigger was a coincidence between an electron and a proton, as described in Ref. [11]. For the measurements at higher  $Q^2$ , at a fixed beam energy of  $4.6 \text{ GeV}$ , the electron was scattered at a larger angle than the proton, and thus defined the rate of the reaction. To maximize the number of elastic events selected, the electron was detected in a calorimeter with a large solid angle. The  $1.35 \times 2.55 \text{ m}^2$  calorimeter was assembled with blocks of lead-glass with a cross-sectional area of  $15 \times 15 \text{ cm}^2$  each, in 9 columns and 17 rows. The use of lead-glass, which produces Čerenkov light, provides good pion background suppression. At each  $Q^2$ , the calorimeter was located at a distance from the target where the electron solid angle matched the proton HRS acceptance according to the Jacobian of the reaction. This distance ranges from 9 m at  $Q^2 = 5.6 \text{ GeV}^2$  to 17 m at  $Q^2 = 4.0 \text{ GeV}^2$ . The trigger was defined by a proton in the HRS, signaled by a coincidence of two planes of scintillators in the focal plane. For each single proton event in the left HRS, the ADC and TDC information from the calorimeter was read out for all blocks, and elastic events were selected by applying software cuts to the calorimeter data. Our analysis showed that the calorimeter registered an ADC signal in about ten blocks for each trigger. A tight coincidence time cut was applied to ensure that the particle detected in the calorimeter came from the same reaction that produced the proton. This considerably reduced that part of the pion electroproduction background for which the scattered electron and the photons from decay of the  $\pi^0$  were mainly not in the acceptance of the calorimeter. A cut was applied to the angular correlation between the proton and the electron to reject events where the pion production products happened to be in the acceptance. The remaining background represents less than 1% of the accepted events, and is taken into account in the polarization analysis, by measuring the polarization of the rejected events. The small bump in the elastic region of the rejected events in Fig. 1 shows that about 5% of elastic events are rejected, because of missing lead-glass

blocks in the calorimeter.

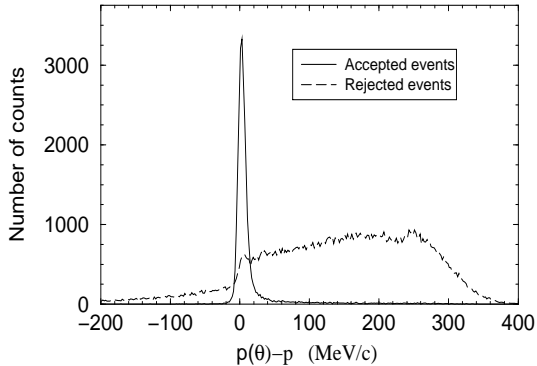


FIG. 1. Selection of elastic events by the calorimeter. The histograms show the spectrum of accepted and rejected events of the momentum difference between the proton momentum expected from its reconstructed scattering angle  $\theta$  and elastic kinematics calculation,  $p(\theta)$ , and its momentum measured by the HRS,  $p$ .

The recoil proton polarization was measured by the focal plane polarimeter (FPP) located behind the focal plane of the left HRS [19]. The FPP determines the two polarization components perpendicular to the momentum,  $P_t^{fpp}$  and  $P_n^{fpp}$ , by measuring asymmetries in the azimuthal angular distribution after scattering the proton in an analyzer. To improve the figure of merit, the usual graphite analyzer was replaced by polyethylene, 60 cm thick at  $Q^2 = 3.5 \text{ GeV}^2$  and 100 cm thick for the other kinematics. The angular distribution is measured by detecting the trajectory of the proton in two sets of two straw chambers, one before and one after the scattering in the analyzer; the distribution is given by:

$$N(\vartheta, \varphi) = N_0(\vartheta) \{1 + [A_y(\vartheta)P_t^{fpp} + a_{in}] \sin \varphi - [A_y(\vartheta)P_n^{fpp} + b_{in}] \cos \varphi\} \quad (2)$$

where  $N_0(\vartheta)$  is the number of protons scattered in the polarimeter to a polar angle  $\vartheta$ ,  $\varphi$  is the azimuthal angle after scattering, and  $A_y(\vartheta)$  is the analyzing power;  $a_{in}$  and  $b_{in}$  are instrumental asymmetries. Such a distribution was measured for the two states of the electron beam helicity, positive and negative. The difference in the beam polarization for these two helicity states was compatible with zero at the 0.3% level [17]. The difference between these two distributions  $N^+/N_0^+ - N^-/N_0^-$  cancels the instrumental asymmetries to first order. It also gives us access to the transferred, helicity-dependent polarization, which is the quantity of interest. The induced, helicity-independent polarization is zero in the case of elastic scattering from the proton. Figure 2 shows this difference distribution, fitted (solid line) with a cosine function  $C \cos(\varphi + \delta)$ , where the amplitude  $C$  is  $\sqrt{(P_n^{fpp})^2 + (P_t^{fpp})^2}$  and the phase shift  $\delta$  is such that

$\tan \delta = P_t^{fpp}/P_n^{fpp}$ . Since  $P_t^{fpp}$  is related to the interference term  $G_{Ep}G_{Mp}$ , this phase shift is a measure of  $G_{Ep}$ . The dashed line represents what the distribution would look like if  $\mu_p G_{Ep}/G_{Mp} = 1$ . The vertical lines at  $\varphi = 90^\circ$  and  $\varphi = 270^\circ$  emphasize the phase shift  $\delta$ .

The proton spin precesses through the magnetic fields of the HRS. The polarization vector at the analyzer of the FPP,  $\mathbf{P}^{fpp}$ , is related to the polarization vector at the target,  $\mathbf{P}$ , by the spin transfer matrix  $\mathbf{S}$ :  $\mathbf{P}^{fpp} = \mathbf{S} \times \mathbf{P}$ . Because protons with different angles and interaction points at the target see different magnetic fields in the HRS, the matrix elements  $S_{ij}$  must be calculated for each event from the reconstructed target coordinates. The matrix elements were determined using a model of the HRS based on optics studies and using the differential algebra-based code COSY [20].

The polarization components  $hA_y P_t$  and  $hA_y P_\ell$  are obtained by maximizing the likelihood function [21]  $L(P_t, P_\ell)$  defined as

$$L(P_t, P_\ell) = \prod_{i=1}^{N_p} \{1 \pm A_y(\vartheta_i)(S_{tt,i}hP_t + S_{t\ell,i}hP_\ell) \sin \varphi_i \mp A_y(\vartheta_i)(S_{nt,i}hP_t + S_{n\ell,i}hP_\ell) \cos \varphi_i\}, \quad (3)$$

where the product runs over all events,  $N_p$ ,  $\pm$  stands for the sign of the beam helicity and  $h$  is the beam polarization. The analyzing power and beam helicity eventually cancel in forming the ratio  $hA_y P_t/hA_y P_\ell$ .

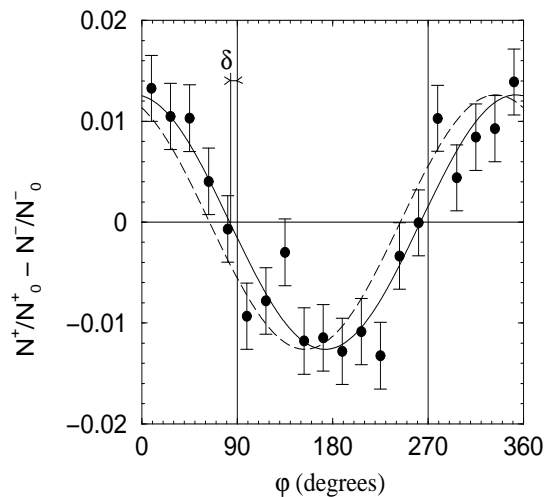


FIG. 2. Difference distribution for positive and negative electron beam helicity, for  $Q^2 = 5.6 \text{ GeV}^2$ . See text for details.

The new results for the ratio  $\mu_p G_{Ep}/G_{Mp}$  are presented in Fig. 3, with statistical error bars, together with the data of Ref. [11]. The systematic errors are represented by the bands at the top. The new data are tabulated in Table I, with their statistical and systematic

errors. The main sources of systematic errors are related to the spin precession. Those can be divided into three parts. Our analysis shows that the major part is the error associated with the uncertainty in the total bending angle in the non-dispersive plane of the spectrometer, due to misalignment of the magnetic elements of the spectrometer. A careful study of this misalignment has been done recently in Hall A [22], reducing the systematic error compared to Ref. [11] at  $Q^2 = 3.5 \text{ GeV}^2$  by a factor of six. The other sources of error in the precession are related to uncertainties in the dipole fringe field model, and to the bending angle in the dispersive plane. Systematic errors associated with proton momentum, electron beam energy and electron scattering angle give smaller contributions. No radiative corrections have been applied to the ratio, as no full calculation of polarization observables for  $ep$  scattering exists. Afanasev *et al.* [23] have calculated the single photon emission corrections to the two polarization observables in hadronic variables. The two corrections are of the same sign, negative, and are each of the order of 1%; thus they largely cancel when one takes the ratio. Other contributions due to two photon-exchange, virtual Compton scattering and interference terms are expected to be at the percent level [24].

A straight line fit has been applied to the ratio  $\mu_p G_{Ep}/G_{Mp}$  in the range  $0.5 < Q^2 < 5.6 \text{ GeV}^2$ :

$$\mu_p \frac{G_{Ep}}{G_{Mp}} = 1 - 0.13(Q^2 - 0.04) \quad (4)$$

Using this  $Q^2$ -dependence as a constraint on  $G_{Ep}$ , the Rosenbluth separation data have been reanalyzed. This brings a correction of the order of 1.5 to 3% to the magnetic form factor [25].

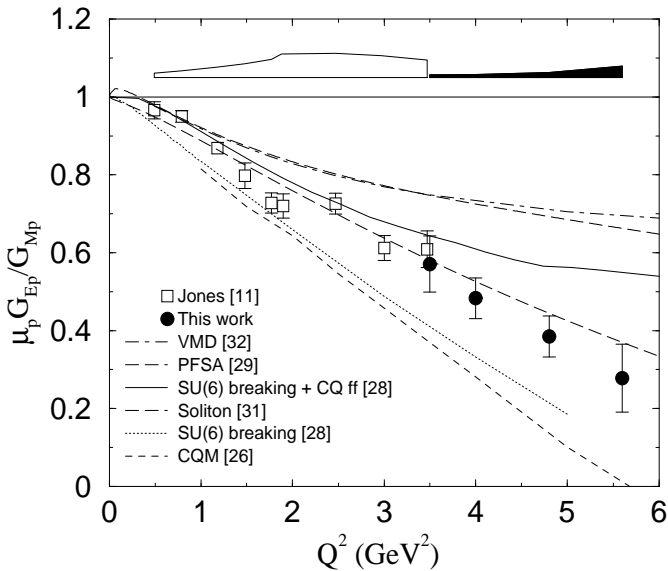


FIG. 3. The ratio  $\mu_p G_{Ep}/G_{Mp}$  from this experiment and Jones *et al.* (Ref. [11]), compared with theoretical calculations. Systematic errors for both experiments are shown as a band at the top of the figure.

Also shown in Fig. 3 are the results of some theoretical calculations which discuss possible interpretations of a decrease of the ratio  $\mu_p G_{Ep}/G_{Mp}$ . Several authors have studied different effects within the framework of the constituent quark model (CQM); all emphasize the necessity of both kinematic and dynamic relativistic corrections. Franck, Jennings and Miller [26], in their study of nuclear medium effects on nucleon electromagnetic form factors, used Schlumpf's light-front wave function in an early relativistic CQM [27] to compute the free proton elastic form factors (dashed curve). Based on the data of Ref. [11], Cardarelli and Simula [28] show that a suppression of the ratio can be expected in the CQM, if the relativistic effects generated by the SU(6) symmetry breaking caused by the Melosh rotations of the constituent spins are taken into account. Their prediction is shown using point-like quark constituents (dotted curve) and constituent quark form factors (solid curve). Wagenbrunn *et al.* [29] (thin long-dashed curve) reach a reasonable agreement with all electroweak nucleon form factors in their point-form spectator approximation (PFSA) prediction of the Goldstone boson exchange CQM [30]. Other types of models try to describe the dynamic features of the nucleon. Holzwarth [31] (thick long-dashed curve) uses a relativistic chiral soliton model, which gives remarkable agreement with the data. Lomon [32] used the world data, including Ref. [11], to perform a fit within the Vector Meson Dominance (VMD) model, where the  $\rho$  meson contribution is determined by dispersion relations (dot-dashed curve). It is worthwhile to note that while some models can reproduce the observed behavior of  $\mu_p G_{Ep}/G_{Mp}$ , they are all based on effective theories and have parameters that can be adjusted to fit the data. No model so far can accurately describe all form factors of the nucleon, as is necessary to fully understand the strong interaction.

The result can also be expressed in terms of the non spin-flip Dirac form factor  $F_{1p}$ , and spin-flip Pauli form factor  $F_{2p}$ , given by:

$$F_{1p} = \frac{G_{Ep} + \tau G_{Mp}}{1 + \tau}; F_{2p} = \frac{G_{Mp} - G_{Ep}}{\kappa_p (1 + \tau)} \quad (5)$$

where  $\kappa_p$  is the anomalous magnetic moment of the proton, and  $\tau = Q^2/4m^2$ . The ratio  $F_{2p}/F_{1p}$  directly follows from  $G_{Ep}/G_{Mp}$ . In Fig. 4a, the results are compared with the pQCD predictions [9] that the asymptotic behavior of the form factors is  $F_{1p} \propto \frac{1}{Q^4}$  and  $F_{2p} \propto \frac{1}{Q^6}$ , so that  $Q^2 \frac{F_{2p}}{F_{1p}}$  would reach a constant value at high enough  $Q^2$ . The data clearly indicate that this asymp-

otic regime has not been reached yet. Based on the results of Ref. [11], Ralston *et al.* [33] postulated a different scaling behavior, where  $F_{2p}/F_{1p}$  goes as  $1/\sqrt{Q^2}$  instead of  $1/Q^2$ , arguing that it corresponds to the pQCD expectation if one takes into account contributions to the proton quark wave-function from states with non-zero orbital angular momentum. The ratio  $\sqrt{Q^2} \frac{F_{2p}}{F_{1p}}$  is shown on Fig. 4b; a constant value is clearly reached starting at  $Q^2 \sim 2 \text{ GeV}^2$ .

In conclusion, we have measured  $G_{Ep}/G_{Mp}$  by polarization transfer to  $Q^2 = 5.6 \text{ GeV}^2$ . The ratio obtained in this experiment continues to decrease, as observed first in Ref. [11]. Extrapolation of the linear trend indicates that the electric form factor would cross zero at  $Q^2 \sim 7.7 \text{ GeV}^2$ . This result also reveals a flattening of the ratio  $QF_{2p}/F_{1p}$  starting at  $Q^2 \sim 2 \text{ GeV}^2$ . A measurement of  $G_{Ep}/G_{Mp}$  to yet higher  $Q^2$  is planned in the near future [34].

The collaboration thanks the Hall A technical staff and the Jefferson Lab Accelerator Division for their outstanding support during the experiment. The Southern Universities Research Association (SURA) operates the Thomas Jefferson National Accelerator Facility for the United States Department of Energy under contract DE-AC05-84ER40150. This work was also supported by the U.S. National Science Foundation and Department of Energy, the Italian Istituto Nazionale di Fisica Nucleare (INFN), the French Commissariat à l'Energie Atomique (CEA) and Centre National de la Recherche Scientifique (CNRS-IN2P3), the Natural Sciences and Engineering Research Council of Canada (NSERC), and the EEC grant INTAS 99-00125 for the Kharkov Institute of Physics and Technology, and CRDF UP2-2271.

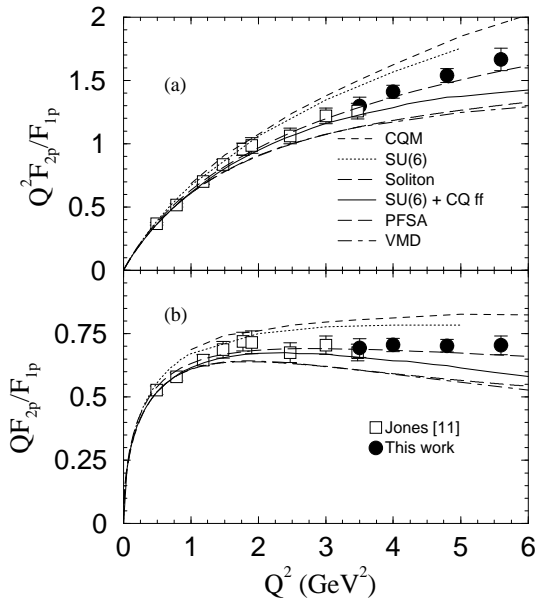


FIG. 4. Same legend as Fig. 3, for (a)  $Q^2 F_{2p}/F_{1p}$  and (b)  $Q F_{2p}/F_{1p}$ .

- 
- [1] M.N. Rosenbluth, Phys. Rev. **79**, 615 (1950).
  - [2] J. Litt *et al.*, Phys. Lett. B **31**, 40 (1970).
  - [3] Ch. Berger *et al.*, Phys. Lett. B **35**, 87 (1971).
  - [4] L.E. Price *et al.*, Phys. Rev. D **4**, 45 (1971).
  - [5] W. Bartel *et al.*, Nuc. Phys. B **58**, 429 (1973).
  - [6] A.F. Sill *et al.*, Phys. Rev. D **48**, 29 (1993).
  - [7] R.C. Walker *et al.*, Phys. Rev. D **49**, 5671 (1994).
  - [8] L. Andivahis *et al.*, Phys. Rev. D **50**, 5491 (1994).
  - [9] S. J. Brodsky and G. P. Lepage, Phys. Rev. D **22**, 2157 (1981).
  - [10] A.I. Akhiezer and M.P. Rekalo, Sov. J. Part. Nucl. **3**, 277 (1974); R. Arnold, C. Carlson and F. Gross, Phys. Rev. C **23**, 363 (1981).
  - [11] M. K. Jones *et al.*, Phys. Rev. Lett. **84**, 1398 (2000); V. Punjabi *et al.*, to be submitted to Phys. Rev. C.
  - [12] B. Milbrath *et al.*, Phys. Rev. Lett. **80**, 452 (1998); erratum, Phys. Rev. Lett. **82**, 2221 (1999).
  - [13] S. Dieterich *et al.*, Phys. Lett. B **500**, 47 (2001).
  - [14] O. Gayou, K. Wijesooriya *et al.*, Phys. Rev. C **64**, 038202 (2001).
  - [15] <http://www.jlab.org/~moller>.
  - [16] N. Fallete *et al.*, Nucl. Instr. and Meth. **A459**, 412 (2001).
  - [17] Stéphanie Escoffier, Thèse de doctorat, CEA Saclay (2001).
  - [18] <http://www.jlab.org/Hall-A/equipment/HRS.html>; B. D. Anderson *et al.*, to be submitted to Nucl. Instr. Meth.
  - [19] M.K. Jones *et al.*, AIP Conf. Proc. **412**, ed. T.W. Donnelly, p. 342 (1997); L. Bimbot *et al.*, to be submitted to Nucl. Instr. Meth.
  - [20] K. Makino and M. Berz, COSY INFINITY version 8, NIM A **427**, 338 (1999).
  - [21] D. Besset *et al.*, Nucl. Instr. Meth. **166**, 512 (1979).
  - [22] L. Pentchev *et al.*, Jlab Technical Note TN-01-052.
  - [23] A. V. Afanasev *et al.*, Phys. Lett. B **514**, 369 (2001).
  - [24] M. P. Rekalo and E. Tomasi-Gustafsson, e-print archive nucl-th/0105002; A. V. Afanasev (private communication).
  - [25] E. J. Brash, A. Kozlov, Sh. Li, G. Huber, to be submitted to Phys. Rev. C., Rapid Communications, October 2001.
  - [26] M. R. Franck, B. K. Jennings and G. A. Miller, Phys. Rev. C **54**, 920 (1995).
  - [27] F. Schlumpf, e-print archive, hep-ph/9405284.
  - [28] F. Cardarelli and S. Simula, Phys. Rev. C **62**, 065201 (2000); S. Simula, e-print archive, nucl-th/0105024.
  - [29] R. F. Wagenbrunn *et al.*, Phys. Lett. B **511**, 33 (2001); e-print archive hep-ph/0108271.
  - [30] L. Ya. Glozman *et al.*, Phys. Rev. D **58**, 094030 (1998).
  - [31] G. Holzwarth, Z. Phys. A **356**, 339 (1996).
  - [32] E. L. Lomon, Phys. Rev. C **64**, 035204 (2001).
  - [33] J. Ralston *et al.*, in Proc. of 7th International Conference on Intersection of Particle and Nuclear Physics, Quebec City (2000), p. 302; private communication (2001).

[34] JLab experiment E01-109, C. F. Perdrisat, V. Punjabi, E. J. Brash and M. K. Jones, spokespersons.

TABLE I. The ratio  $\mu_p G_{Ep}/G_{Mp}$  with statistical uncertainty ( $1\sigma$ )  $\Delta_{stat}$ , and systematic uncertainty  $\Delta_{sys}$ .  $\langle Q^2 \rangle$  is the value of  $Q^2$  weighted-averaged over the acceptance, and  $\Delta Q^2$  is the  $Q^2$  acceptance ( $1\sigma$ ).

$\langle Q^2 \rangle \pm \Delta Q^2$ (GeV <sup>2</sup> )	$\mu_p G_{Ep}/G_{Mp}$	$\Delta_{stat}$	$\Delta_{sys}$
3.50±0.23	0.571	0.072	0.007
3.97±0.26	0.483	0.052	0.008
4.75±0.30	0.385	0.053	0.011
5.54±0.34	0.278	0.087	0.029